Differential elastic and total electron scattering cross sections of tetrahydrofuran

W. Y. Baek,[1] M. Bug,[1] H. Rabus,[1] E. Gargioni,[2] and B. Grosswendt[3]
[1]*Physikalisch-Technische Bundesanstalt, Bundesallee 100, 38116 Braunschweig, Germany*
[2]*University Medical Center Hamburg-Eppendorf, Martinistrasse 52, 20246 Hamburg, Germany*
[3]*Weissdornstrasse 65A, 31228 Peine, Germany*
(Received 21 March 2012; published 4 September 2012)

Differential elastic scattering cross sections of tetrahydrofuran for electrons were measured absolutely in the energy range from 20 eV to 1 keV at scattering angles between 5° and 135°. The measurements were carried out using a crossed-beam arrangement without the application of the widely used relative flow technique. The experimental differential scattering cross sections could be put on an absolute scale by means of the total electron scattering cross sections of tetrahydrofuran and of the current loss of the primary electron beam in the forward direction arising due to the scattering by the molecular beam. The total scattering cross sections were determined for electron energies between 6 eV and 1 keV using a separate linear transmission experiment. The differential cross sections of tetrahydrofuran for the elastic scattering of electrons were also calculated in the energy range between 60 eV and 1 keV by applying the modified independent-atom model. A comparison with the experimental results showed a satisfactory agreement, indicating that the selected theoretical model is adequate for these calculations.

DOI: 10.1103/PhysRevA.86.032702 PACS number(s): 34.80.Bm

I. INTRODUCTION

Radiobiological investigations have hitherto suggested that DNA is the critical radiosensitive target within a cell. The inactivation or mutation of a cell can be generally attributed to biological damage to DNA in the form of double strand breaks or multiple base damages. This damage may arise due to a direct excitation and ionization of DNA constituents by primary radiation or secondary particles or by indirect processes such as the reaction of DNA with hydroxyl radicals produced by the interaction of ionizing radiation with water.

Electrons are produced in a large number as secondary particles by any kind of ionizing radiation penetrating matter. The majority of the secondary electrons have energies below 1 keV. These low-energy electrons have small ranges, typically in the order of the diameter of the DNA, and therefore significantly contribute to the production of clustered damages in the DNA. Since the track structure of electrons on a nanometric scale is experimentally difficult to observe, Monte Carlo simulations are commonly used to trace the electron paths and to study their action on DNA. Such studies, however, require knowledge of the electron scattering cross sections of DNA constituents.

While interaction cross sections of water for electrons have been subject to extensive investigations, only a few experimental data have been published for those of DNA constituents. Milosavljevic *et al*. [1] measured differential elastic scattering cross sections (DCS) of tetrahydrofuran (THF), which has a structure similar to the deoxyribose in the DNA backbone and therefore is used as its model molecule, for electron energies between 20 and 300 eV. Colyer *et al*. [2] and Dampc *et al*. [3] determined the DCS of THF in the energy range from 6.5 to 50 eV and from 6 to 20 eV, respectively. In addition to the DCS, Allan [4] reported vibrational excitation cross sections of THF for electron energies below 20 eV. Recently, Homem *et al*. [5] published rather comprehensive data sets covering the DCS of THF for electron energies from 50 to 1000 eV in the angular range between 5° and 130°. Experimental total electron scattering cross sections (TCS) have been reported by Zecca *et al*. [6] for electron energies from 2 to 21 eV and by Możejko *et al*. [7] for electron energies from 1 to 370 eV. Fuss *et al*. [8] reported the TCS of THF in the energy range between 50 eV and 5 keV.

There are, however, large discrepancies between the experimental data of different groups. For instance, the TCS of THF reported by Możejko *et al*. [7] are about 50% higher than those of Zecca *et al*. [6]. Similar or even larger deviations can also be observed in the case of the DCS of THF. In view of this fact, the TCS of THF were absolutely measured in the present work for electron energies from 6 eV to 1 keV, and the DCS of THF from 20 eV to 1 keV for scattering angles between 5° and 135°.

II. PRINCIPLE OF DCS MEASUREMENT

A. Limits of the relative flow technique

One of the major problems arising in the measurement of DCS using a crossed-beam arrangement is the determination of the interaction volume between the electron and the molecular beam. In the early 1980s, Brinkmann and Trajmar [9] conducted a detailed investigation regarding the influence of scattering geometry on the results of a crossed-beam experiment. Following their notation, the relationship between the count rate $\Delta\dot{N}_{\mathrm{el}}(\theta)$of elastically scattered electrons and the DCS $d\sigma_{\mathrm{el}}(\theta)/d\Omega$, averaged over all molecular orientations, is given by

$$\Delta\dot{N}_{\mathrm{el}}(\theta,T) = \eta(T)\frac{d\sigma_{\mathrm{el}}(\theta,T)}{d\Omega}V_{\mathrm{eff}}, \tag{1}$$

where $\eta(T)$ is the detection efficiency for electrons of energy T and V_{eff} is defined by

$$V_{\mathrm{eff}} = \int_V i(\vec{r})f(\vec{r})\Delta\Omega(\vec{r})G[\theta'(\vec{r})]d^3r. \tag{2}$$

In Eq. (2), $i(\vec{r})$ and $f(\vec{r})$ are the spatial distribution of the electron flux and of the density of target molecules,

respectively, and $\Delta\Omega(\vec{r})$ is the solid angle of the detector viewed at the position $\vec{r}$ within the scattering volume V. $G[\theta'(\vec{r})]$ accounts for the change of the DCS due to the variation of the scattering angle within the scattering volume. In the derivation of Eqs. (1) and (2), it was assumed that the responsitivity of the detector is independent of the scattering angle and target molecules are oriented randomly, so that the DCS is independent of the azimuthal angle.

According to Eq. (1), the value of V_{eff} must be accurately known for a precise determination of the absolute DCS. Since the determination of V_{eff} is, however, very difficult in practice, the DCS is commonly measured by employing the relative flow technique [10]. In this technique, the DCS of the gas of interest is measured relative to that of a reference gas whose cross section is well known. In most cases, the DCS of helium is used as the reference cross section.

The relative flow technique [10] is based on the assumption that the beam profiles of the reference gas and of the gas of interest are identical if the pressures in the reservoir over the beam-generating gas tube are chosen such that the mean free paths for interatomic or intermolecular collisions in the gas tube are the same for both gases. This means that the application of the relative flow technique [10] requires the knowledge of the cross section of intermolecular collisions, which is inversely proportional to the mean free path. The cross section for intermolecular collisions is, however, not known for a great part of complex organic molecules and therefore, an approximate value is often used. For instance, Dampc *et al*. [3] employed the average molecular diameter of the ethoxy ethane molecule to determine the collisional mean free path for THF in applying the relative flow technique [10]. Moreover, Buckman *et al*. [11] suggested that the profile of a helium beam and other gas beams might be significantly different even at equivalent mean free paths if the pressure in the gas tube is comparable to or higher than that of the free molecular flow regime which sets a limit to the gas pressure and, consequently, to the signal-to-noise ratio in the scattering experiment.

B. Derivation of the present experimental method

In view of the limits of the relative flow technique, an experimental method was developed to absolutely measure the DCS of complex organic molecules without employing a reference cross section. The main feature of this method is the determination of V_{eff} by means of the current loss ΔI of the primary electron beam after passage through the molecular beam and the knowledge of the TCS σ_t, which can be more accurately measured. The derivation of the basic equation used in this method is described in the Appendix.

According to Eq. (A10), five quantities are required for the determination of the DCS: the detection efficiency $\eta(T)$ as a function of the electron energy T, the solid angle $\Delta\Omega$ subtended by the detector, the measured count rate $\Delta\dot{N}_{\text{el}}(\theta,T)$ of elastically scattered electrons as a function of the scattering angle θ, the TCS $\sigma_t(T)$, and the current loss ΔI of the primary electron beam in the forward direction due to the scattering by the molecular beam.

In the present work, an electrostatic hemispherical electron energy analyzer with a mean radius and deflection angle of 150 mm and 180°, respectively, was employed to measure the count rate $\Delta\dot{N}_{\text{el}}(\theta,T)$of elastically scattered electrons, using a channel electron multiplier as detector. The electron detection efficiency $\eta(T)$ is composed of the transmittance $\eta_1(T)$ of the energy analyzer and the responsitivity $\eta_2(T)$ of the channel electron multiplier:

$$\eta(T) = \eta_1(T)\eta_2(T). \tag{3}$$

To determine $\eta(T)$, the energy dependence of the transmittance of the electron energy analyzer was at first calculated numerically by the simulation of electron paths through the energy analyzer. For this purpose, the electric field distribution in the electron energy analyzer was computed by solving the Laplace equation for the voltages applied to the path-influencing electrodes of the energy analyzer. The path of electrons moving in this electric field distribution was then traced from the scattering area to the detector. The path calculation was carried out for electrons of different energies elastically scattered by He at 90°. All the voltages influencing the electron path were changed proportionally to the electron energy in agreement with the operating condition of the electron energy analyzer used in the present work and with the scaling law for charged particle motion in static electric fields [12].

The angular distribution of electrons leaving the scattering area was determined by the interpolation of experimental DCS of He [13] for electron energies below 200 eV, while that above 200 eV was obtained from the Electron Elastic-Scattering Cross-Section Database of NIST [14]. Since not the absolute value of the DCS but only their angular dependence over a small angle range around 90° is of relevance for this purpose, and the DCS of He in this angular range is a smooth function of the scattering angle over the energy region of interest for this work, the uncertainty arising due to this interpolation is negligibly small compared to other uncertainties discussed below. The theoretical transmittance was then determined by the calculation of the ratio of the number of electrons entering the analyzer to that reaching the detector after traveling through the hemispherical deflector. The relative energy dependence $\hat{\eta}_1(T)$ of the theoretical analyzer transmittance was defined as the ratio of $\eta_1(T)$ to its value at 20 eV: $\hat{\eta}_1(T) = \eta_1(T)/\eta_1(T = 20\text{ eV})$.

In order to verify the accuracy of the electron-path calculation, the shape of the elastic scattering peak was calculated for different potential distributions in the energy analyzer and compared with the experimental data. The electrical potential distribution in the energy analyzer was varied by applying a retardation voltage to the entrance area of the hemispherical deflector. This retardation voltage leads to a de-acceleration of incoming electrons which then move with a reduced energy through the hemispherical deflector so that lower analyzer pass energy is required to transmit the electrons. The retardation method [12] is often used to improve the energy resolution of electron energy analyzers. Figures 1(a) and 1(b) show the dependence of the count rate of 1 keV electrons scattered elastically by He on the analyzer pass energy for two retardation voltages of 990 and 900 V, respectively. It can be seen from Figs. 1(a) and 1(b) that the calculated shape of the elastic scattering peak agrees reasonably well with the experimental observation. The voltage difference across the

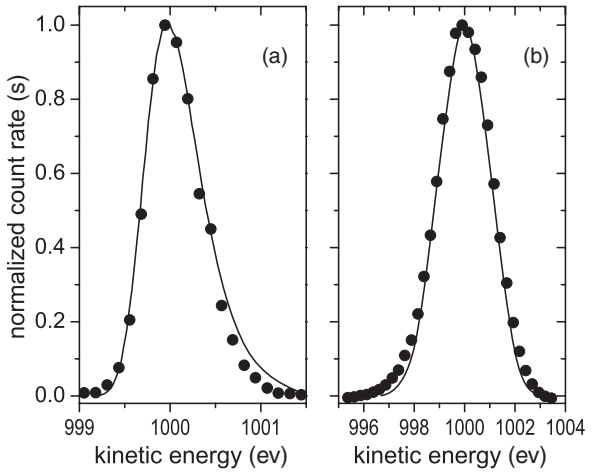

FIG. 1. Experimental (•) and theoretical (−) count rate of 1 keV electrons scattered elastically by helium at the scattering angle of 90° as a function of the kinetic energy for two pass energies: (a) 10 eV and (b) 100 eV. The peak heights were normalized to unity.

hemispherical deflector, and consequently the electric field in the deflector, depend only on the analyzer pass energy; in other words, electrons with an initial energy T and a reduced kinetic energy T_1 after the retardation move on the same trajectory as those with an initial kinetic energy T_1 with no retardation. Therefore, the good agreement between the experimental and theoretical peak shapes in Figs. 1(a) and 1(b) suggests that the relative energy dependence $\hat{\eta}_1(T)$ of the analyzer transmittance is realistic for electron energies down to around 10 eV. It should be noted that the two experimental results in Figs. 1(a) and 1(b) were obtained by using the same atomic and electron beam so that the peak shape was not affected by any change of the beam profiles.

The responsitivity η_2 of the channel electron multiplier was measured by operating it additionally in an analog mode [15] and by comparing the current collected in this mode with the count rate obtained in the pulse counting mode [15] while keeping the primary electron-beam current as well as the molecular flow rate constant. To avoid the change of the responsitivity of the channel electron multiplier on the count rate that occurs at high count rates, the count rates were kept below 10^4/s. As the currents corresponding to these count rates are too low to be determined with sufficient accuracy, the count rate of the channel electron multiplier was measured for 2000 s. The responsivity η_2 of the channel electron multiplier was then determined as the ratio of the integrated count rate to the charge collected in the same time interval. The relative energy dependence $\hat{\eta}_2(T)$of the detector responsitivity is given again by $\hat{\eta}_2(T) = \eta_2(T)/\eta_2(T = 20\ \text{eV})$, where $\eta_2(T = 20\ \text{eV})$ is the detector responsitivity for 20 eV electrons.

The absolute value of $\eta(T) = \eta_1(T) \times \eta_2(T)$ was obtained by the multiplication of $\hat{\eta}(T) = \hat{\eta}_1(T) \times \hat{\eta}_2(T)$ with the detection efficiency $\eta(T = 20\ \text{eV})$ for 20 eV electrons, which was determined by means of the electron scattering cross section of helium at that energy. Apart from the optically forbidden transition $1\,^1S \rightarrow 2\,^3S$ at 19.8 eV, the scattering of 20 eV electrons by He is entirely of an elastic nature. As the cross section for the transition $1\,^1S \rightarrow 2\,^3S$ in He by 20 eV electrons is about two orders of magnitude smaller than

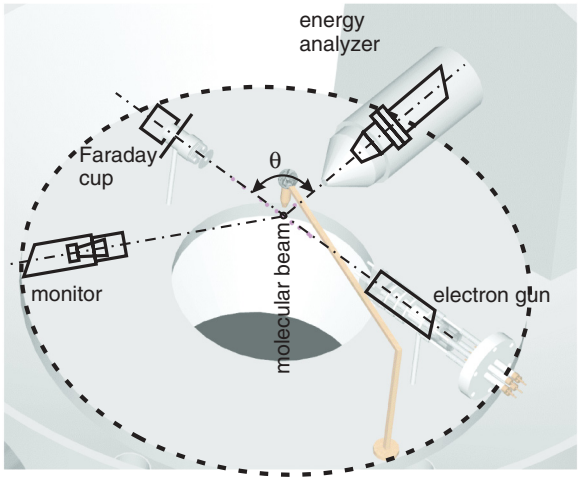

FIG. 2. (Color online) Schematic view of the experimental setup used for the measurement of the DCS in the scattering plane. The flow direction of the molecular beam is perpendicular to that of the electron beam and to the normal of the entrance plane of the hemispherical deflector. The scattering angle was adjusted by the rotation of the electron gun, and the beam stability monitor, a channel electron multiplier, was mounted at a distance of 15 cm from the scattering volume and at an angle of 15° relative to the electron-beam direction.

the integral elastic scattering cross sectionσ_{el} of He at that energy [16,17], σ_{el} is almost equal to the TCS σ_t:

$$\sigma_t \approx \sigma_{\text{el}} = \int \frac{d\sigma_{\text{el}}(\theta)}{d\Omega} d\Omega = \int \frac{e}{\eta} \frac{\Delta \dot{N}_{\text{el}}(\theta)}{\Delta\Omega} \frac{\sigma_t}{\Delta I} d\Omega, \quad (4)$$

where $\Delta \dot{N}_{\text{el}}(\theta)$ is the count rate of the elastic scattering peak at the scattering angle θ, σ_t is the total electron scattering cross section, and ΔI is the electron current loss due to scattering.

If the experiment is performed under the condition that the current loss ΔI does not change with the scattering angle θ, Eq. (4) is equivalent to

$$\Delta I = \int \frac{e}{\eta} \frac{\Delta \dot{N}_{\text{el}}(\theta)}{\Delta\Omega} d\Omega. \quad (5)$$

Equation (5) was used to determine the experimental value of the detection efficiency $\eta(T = 20\ \text{eV})$ for 20 eV electrons. For this purpose, the count rate $\Delta \dot{N}(\theta)$ of 20 eV electrons scattered by helium was measured in the angular range between 15° and 140° using the experimental setup depicted in Fig. 2 and described below. The scattering angle was adjusted by rotating the electron gun while the energy analyzer was fixed in position. To prevent alterations in ΔI when changing the scattering angle, both the gas tube and the electron gun were mounted on a turntable so that they rotated together around the same axis when changing the scattering angle. Therefore, the intersection volume between the electron beam and the molecular beam, and consequently the current loss ΔI, was independent of the scattering angle in the first order. A possible variation of ΔI due to instabilities of the electron and molecular beam was corrected with the help of the beam stability monitor (see below).

The count rates per solid angle $\Delta \dot{N}_{\text{el}}(\theta)/\Delta\Omega$ for scattering angles below 15° and above 140° were determined by the

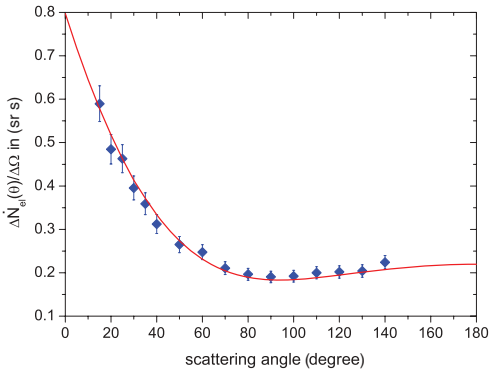

FIG. 3. (Color online) Angular dependence of $\Delta\dot{N}_{\rm el}(\theta)/\Delta\Omega$ (♦) of 20-eV electrons scattered elastically by He. It was normalized to the DCS (−) of He proposed by Register *et al*. [13] at the scattering angle of 25°.

extrapolation of the measured data using the DCS of He proposed by Register *et al*. [13], which are commonly taken as the reference cross sections in experiments applying the relative flow technique [10] along with the analytical fit formula of Boesten and Tanaka [18]. As Fig. 3 shows, the angular dependence of $\Delta\dot{N}_{\rm el}(\theta)/\Delta\Omega$ measured in the present work agrees with that of the DCS of Register *et al*. [13] within the experimental uncertainties. It is therefore assumed that both follow the same angular dependence also at scattering angles below 15° and above 140°.

Since $\Delta\dot{N}_{\rm el}(\theta)/\Delta\Omega$ was known for the whole angular range, it was numerically integrated to determine the experimental value of the detection efficiency $\eta(T = 20\ \text{eV})$ for 20 eV electrons according to Eq. (5):

$$\eta(T = 20\ \text{eV}) = \frac{\int \frac{e\Delta\dot{N}_{\rm el}(\theta, T=20\ \text{eV})}{\Delta\Omega} d\Omega}{\Delta I}. \tag{6}$$

The detection efficiency $\eta(T)$ for other electron energies was finally obtained by multiplying $\hat{\eta}(T)$ with $\eta(T = 20\ \text{eV})$:

$$\eta(T) = \hat{\eta}(T)\eta(T = 20\ \text{eV}). \tag{7}$$

It is worthwhile noting that the detection efficiency $\eta(T = 20\ \text{eV})$ obtained using the data of Register *et al*. [13] and the fit formula of Boesten and Tanaka [18] for the extrapolation of the DCS of He for scattering angles below 15° and above 140° differ from each other <0.5%.

In the present work, the DCS of THF were measured using $\eta(T)$ determined in this way in combination with Eq. (A10):

$$\frac{d\sigma_{\rm el}}{d\Omega}(\theta, T) = \frac{e}{\eta(T)} \frac{(\Delta\dot{N}_{\rm el})}{\Delta\Omega}(\theta, T) \frac{\sigma_t(T)}{\Delta I(T)}. \tag{8}$$

It should be mentioned that the application of Eq. (6) induces a correlation between the detection efficiency $\eta(T)$ and the solid angle Ω. A solid angle lower than the true value would lead to a proportional decrease of $\eta(T)$ and vice versa so that the absolute scale of the DCS determined using Eq. (8) is not affected by a possible inaccuracy of the solid angle.

III. MEASUREMENT OF DCS OF THF

A. Experimental setup

The apparatus used for the measurement of the DCS of THF was the same as that used above to collect the count rate of electrons scattered elastically by He. The schematic view of the experimental setup in the scattering plane, which is defined by the electron-beam direction and the symmetry axis of the energy analyzer, is shown in Fig. 2. Electrons were produced by an electron gun which delivered a well-focused electron beam for electron energies from 20 eV to 1 keV with an energy width (FWHM) of ∼0.5 eV. The electron gun was mounted on a turntable enabling the adjustment of the scattering angle.

The molecular beam was generated by a single tube 80 mm in length and 2 mm in diameter. It was orthogonally crossed by the electron beam 1 mm below the exit of the gas tube. The electron-beam current after its passage through the molecular beam was measured by a Faraday cup placed opposite to the electron gun. In order to avoid any change of intersection area between the electron and molecular beam with the scattering angle due to a potentially imperfect alignment, the gas tube was mechanically joined to the electron gun so that both rotated together during the adjustment of the scattering angle. In order to monitor the stability of the electron beam and the molecular flow, a channel electron multiplier was mounted at a fixed angle relative to the electron-beam direction and continuously counted the electrons scattered into a fixed solid angle.

The primary beam current was kept between 1.0 pA and 1.0 nA, depending on the electron energy. In general, the electron-beam current was raised at high electron energies because of the decrease of elastic scattering cross sections with increasing energy. Tetrahydrofuran was purchased from Aldrich Chemical Ltd. The purity stated by the manufacturer was 99%. The gas flow rate through the molecular beam tube was ∼0.1 mbar l/s. It could be adjusted by means of a leak valve built in between the reservoir above the gas tube and the bottle containing liquid THF. The vapor pressure of THF, which amounts to 173 mbar at 20 °C was sufficiently high for the purpose of this experiment, so that no heating of the liquid and gas line was necessary.

The driving pressure above the gas tube was measured by means of a capacitance manometer. Its typical value amounted to 0.5 mbar. If the average molecular diameter of an ethoxy ethane molecule, 4.63 Å, is used as the collision diameter of THF as was done by Dampc *et al*. [3], the mean free path λ_c for intermolecular collisions at the entrance of the gas tube amounts to 1.5 mm, leading to Knudsen numbers $K_D = \lambda_c/D_T < 1$ and $K_L = \lambda_c/L_T < 1$, where D_T and L_T are the diameter and length of the gas tube, respectively. This means that the gas effusion did not take place in the molecular but rather in the intermediate flow region.

The number of molecules per area hit by the electron beam at a gas pressure of 0.5 mbar in the reservoir was estimated as $\sim 5 \times 10^{13}/\text{cm}^2$. The gas pressure was chosen such that it is sufficiently high to cause a relative current loss of at least 3% but at the same time low enough to fulfill the single collision condition.

The scattering chamber was made of permalloy 8 mm in thickness in order to shield against the Earth's magnetic field. In this way, the magnetic field strength in the scattering area

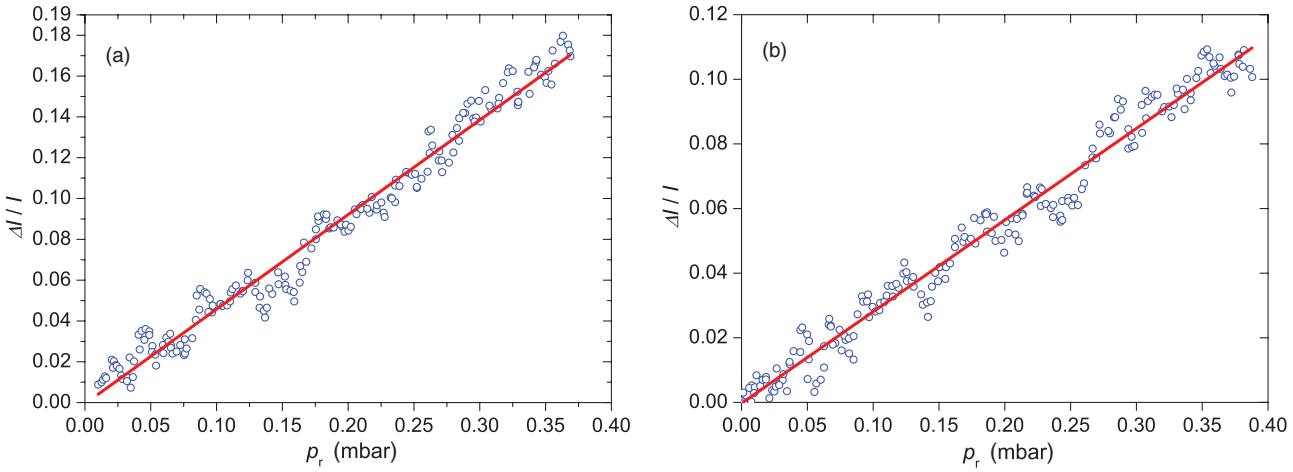

FIG. 4. (Color online) Dependence of the current loss ΔI(◯) on the gas pressure p_r in the reservoir over the gas tube and the best line fit (−) to $\Delta I/I$ vs p_r for two electron energies: (a) 20 eV and (b) 100 eV.

was reduced to a value smaller than 10^{-6} tesla. The scattered electrons entered the hemispherical deflector through a slit 3 mm in width and 20 mm in height. As mentioned above, the hemispherical deflector had a mean radius of 150 mm and a deflection angle of 180°.

B. Measurement of the elastic scattering count rate

The energy spectra of scattered electrons were obtained by recording the detector count rate as a function of the kinetic energy, where the measured count rate of the elastically scattered electrons $\Delta\dot{N}_{\rm el}(\theta,T)$ was defined as the area under the elastic scattering peak in the energy spectra. The angular resolution of the energy analyzer could be adjusted by means of an iris aperture located between the scattering area and the entrance slit of the hemispherical deflector. For the scattering angles above 35° where the DCS of THF show a rather smooth angular dependence, the half angle of acceptance amounted to 1.5°, while it was adjusted to <0.8° for the scattering angles below 35°. The accuracy of the angle positioning of the electron gun was checked by means of the DCS of Ar for 100 eV electrons, the angular dependence of which exhibits a sharp minimum at the scattering angle of around 123°. The position of the peak measured using the present apparatus agreed with that of the theoretical prediction [14] within the angular resolution mentioned above.

The energy resolution (FWHM) of the energy analyzer, which can be adjusted by varying the retardation voltage [12], amounted to 1.7 eV for 1 keV electrons and was better at lower energies. It should be noted that the energy resolution of 1.7 eV is not sufficient to resolve between the elastic scattering and rotational excitations; in other words, the elastic scattering peaks at high energies include contributions by rotational excitations.

Due to the gas flow, the background pressure in the scattering chamber increased from 5.0×10^{-7} mbar to 5.0×10^{-5} mbar at a pumping speed of 1900 l/s. The energy analyzer was differentially evacuated by an additional turbomolecular pump with a pumping speed of 250 l/s, so that the residual pressure in the energy analyzer was kept smaller than 3.0×10^{-6} mbar during the measurements.

Two runs of measurements were performed for each scattering angle and energy. The second run was carried out to determine the contribution of electrons scattered by the background gas and metallic surfaces to the area under the elastic scattering peak. For this purpose, THF was not introduced through the gas tube but diffusely through a wide hole. The rate of the gas introduction was chosen such that the gas pressure in the chamber was equal to the background pressure arising due to the molecular beam in the first run of the measurement. The area $\Delta\dot{N}_{\rm el}^{(2)}(\theta,T)$ of the elastic scattering peak measured in the second run was then subtracted from that measured in the first run, $\Delta\dot{N}_{\rm el}^{(1)}(\theta,T)$, to obtain the net elastic scattering count rate $\Delta\dot{N}_{\rm el}(\theta,T)$ without the contribution of background electrons:

$$\Delta\dot{N}_{\rm el}(\theta,T) = \Delta\dot{N}_{\rm el}^{(1)}(\theta,T) - \Delta\dot{N}_{\rm el}^{(2)}(\theta,T)\frac{I_1}{I_2}, \qquad (9)$$

where I_1 and I_2 are the primary electron-beam currents in the first and second run of the measurement, respectively. The net count rate $\Delta\dot{N}_{\rm el}(\theta,T)$ was then inserted into Eq. (8) to determine the DCS.

C. Measurement of the primary beam current loss

A quantity that critically influences the accuracy of the measurement but is sensitive to distortion effects, such as the leakage current and electromagnetic noise, is the current loss ΔI. It was therefore carefully measured using a Faraday cup with a deep and narrow hole in combination with electrostatic guide rings to prevent secondary electrons from escaping the cup. To reduce the uncertainty arsing due to statistical fluctuations, it was collected usually more than 100 times during the measurement of the elastic scattering peak and an average value of the collected data was employed in the determination of the DCS.

In order to check the magnitude of the distortion effects, the current loss was measured as a function of the driving pressure p_r in the reservoir above the gas tube for each scattering angle and energy, before the measurement of the elastic scattering count rate. In ideal experimental conditions, where

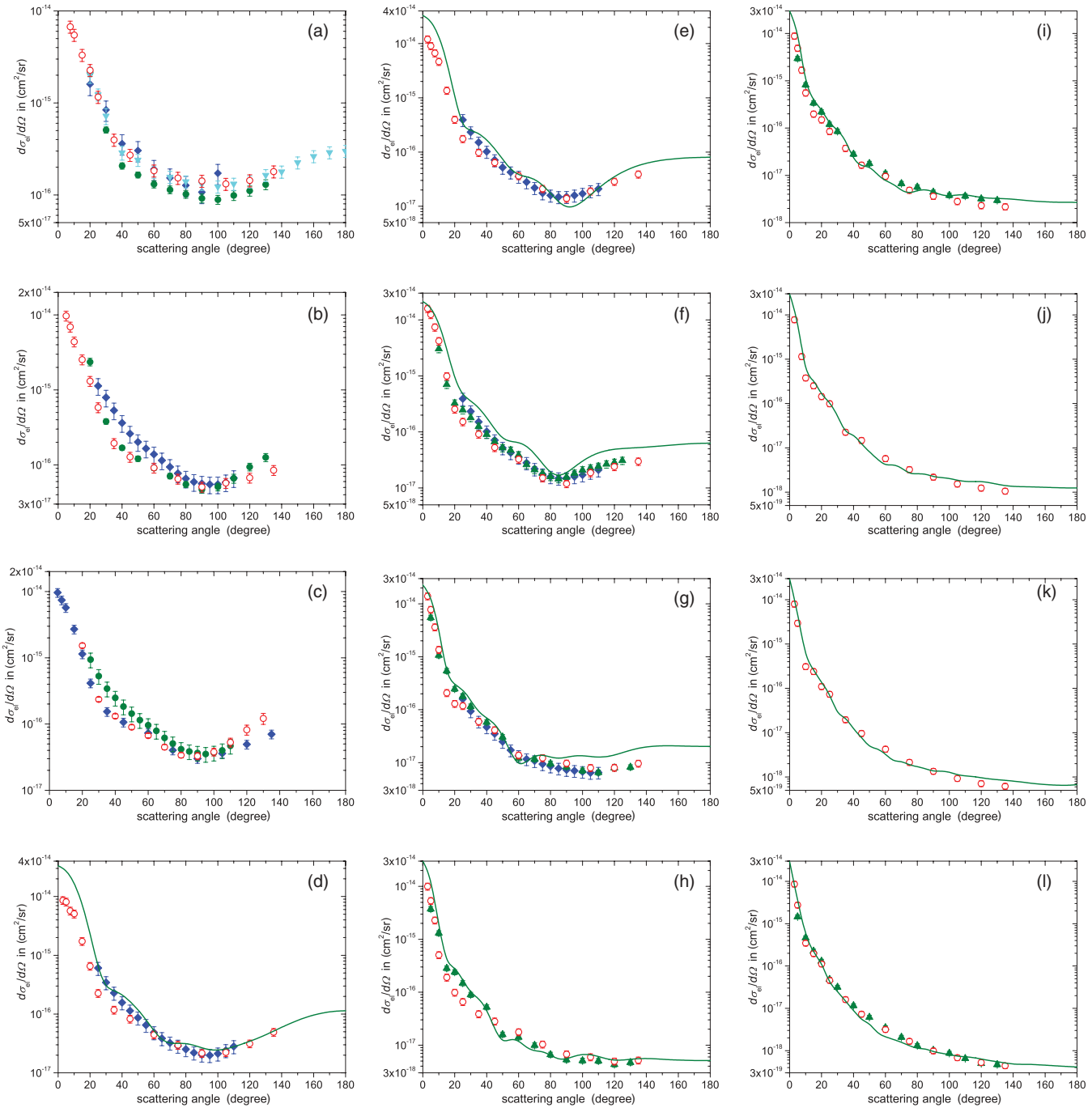

FIG. 5. (Color online) Present results (◯) of the DCS of THF in comparison to the experimental data of Milosavljevic *et al*. [1] (♦), Colyer *et al*. [2] (●), Dampc *et al*. [3] (▼), and Homem *et al*. [5] (▲), and to the theoretical values (−) obtained using the modified independent-atom model [23] for different electrons energies: (a) 20 eV, (b) 30 eV, (c) 40 eV, (d) 60 eV, (e) 80 eV, (f) 100 eV, (g) 200 eV, (h) 300 eV, (i) 400 eV, (j) 600 eV, (k) 800 eV, and (l) 1000 eV.

no secondary distortion effects are present, it is to be expected that the current loss increases linearly with the driving pressure p_r and the gradient of the increase is proportional to the TCS. Figures 4(a) and 4(b) show examples of the measurement for 20 and 100 eV electrons. In the above examples, the relative uncertainty of a least-square line fitting to ΔI vs p_r amounts to ∼1%. Furthermore, the ratio of the best-fit line slopes for both energies differs from that of the TCS by ∼4%, which is in the order of the experimental uncertainty. At other energies, the relative difference between both ratios did not exceed 7%.

IV. RESULTS AND DISCUSSION OF EXPERIMENTAL DCS

The experimental results are listed in Table I and displayed in Figs. 5(a)–5(l) in comparison to the data of other experimental groups and to the theoretical values calculated

TABLE I. Differential elastic electron scattering cross sections of THF as a function of the scattering angle for different energies. The cross sections are given in units of 10^{-16} cm^2/sr. Numbers in parentheses are powers of ten that multiply the cross sections as well as the uncertainties.

	Electron energy			
Scattering angle	20 eV	30 eV	40 eV	60 eV
3°				86.29 ± 12.77
5°		97.47 ± 14.43	96.37 ± 14.27	81.35 ± 12.04
7.5°	67.34 ± 9.97	69.52 ± 10.29	74.11 ± 10.97	57.06 ± 8.44
10°	54.84 ± 8.12	44.10 ± 6.53	57.05 ± 8.44	50.86 ± 7.53
15°	33.15 ± 4.81	25.44 ± 3.69	27.03 ± 3.87	17.33 ± 2.44
20°	22.73 ± 3.30	13.14 ± 1.91	11.40 ± 1.63	6.56 ± 0.92
25°	11.62 ± 1.68	5.84 ± 0.85	4.14 ± 0.59	2.26 ± 0.32
35°	3.97 ± 0.58	1.95 ± 0.28	1.54 ± 0.22	1.18 ± 0.17
45°	2.72 ± 0.39	1.28 ± 0.19	1.06 ± 0.15	8.28 ± 1.17(−1)
60°	1.84 ± 0.27	9.15 ± 1.33(−1)	7.32 ± 1.05(−1)	4.47 ± 0.63(−1)
75°	1.53 ± 0.22	6.51 ± 0.94(−1)	4.03 ± 0.58(−1)	2.97 ± 0.42(−1)
90°	1.42 ± 0.21	5.08 ± 0.74(−1)	3.01 ± 0.43(−1)	2.16 ± 0.30(−1)
105°	1.32 ± 0.19	5.73 ± 0.83(−1)	3.61 ± 0.52(−1)	2.23 ± 0.31(−1)
120°	1.44 ± 0.21	6.73 ± 0.98(−1)	4.93 ± 0.71(−1)	3.14 ± 0.44(−1)
135°	1.80 ± 0.26	8.52 ± 1.23(−1)	7.02 ± 0.10(−1)	4.93 ± 0.69(−1)
	Electron energy			
Scattering angle	80 eV	100 eV	200 eV	300 eV
3°	120.4 ± 17.82	158.7 ± 23.49	139.9 ± 20.71	90.89 ± 13.45
5°	90.97 ± 13.19	123.8 ± 17.95	77.89 ± 11.53	48.55 ± 7.19
7.5°	66.93 ± 9.70	73.91 ± 10.57	36.36 ± 5.27	20.8 ± 3.02
10°	46.51 ± 6.74	41.99 ± 5.61	13.66 ± 1.95	4.60 ± 0.66
15°	13.64 ± 1.90	9.91 ± 1.36	2.08 ± 0.29	9.48 ± 1.29(−1)
20°	3.97 ± 0.55	2.54 ± 0.35	1.30 ± 0.18	9.02 ± 1.23(−1)
25°	1.76 ± 0.24	1.52 ± 0.21	1.19 ± 0.16	5.99 ± 0.81(−1)
35°	9.78 ± 1.36(−1)	9.13 ± 1.25(−1)	5.98 ± 0.82(−1)	3.52 ± 0.48(−1)
45°	6.41 ± 0.89(−1)	5.25 ± 0.72(−1)	4.14 ± 0.57(−1)	2.57 ± 0.35(−1)
60°	3.64 ± 0.51(−1)	3.25 ± 0.45(−1)	1.38 ± 0.19(−1)	1.61 ± 0.22(−1)
75°	2.11 ± 0.29(−1)	1.51 ± 0.21(−1)	1.23 ± 0.17(−1)	9.43 ± 1.28(−2)
90°	1.40 ± 0.19(−1)	1.19 ± 0.16(−1)	9.70 ± 1.33(−2)	6.16 ± 0.84(−2)
105°	1.89 ± 0.26(−1)	1.87 ± 0.26(−1)	8.01 ± 1.10(−2)	5.42 ± 0.74(−2)
120°	2.86 ± 0.40(−1)	2.40 ± 0.33(−1)	8.06 ± 1.11(−2)	4.50 ± 0.61(−2)
135°	3.90 ± 0.54(−1)	2.98 ± 0.41(−1)	9.67 ± 1.33(−2)	4.70 ± 0.06(−2)
	Electron energy			
Scattering angle	400 eV	600 eV	800 eV	1000 eV
3°	88.49 ± 1310	78.25 ± 11.58	80.20 ± 11.87	86.56 ± 12.81
5°	49.02 ± 7.25		29.59 ± 4.38	27.62 ± 4.09
7.5°	16.88 ± 2.45	11.49 ± 1.64		
10°	5.57 ± 0.80	3.80 ± 0.54	3.12 ± 0.44	3.50 ± 0.49
15°	1.98 ± 0.27	2.53 ± 0.34	2.41 ± 0.32	1.97 ± 0.26
20°	1.50 ± 0.20	1.45 ± 0.20	1.11 ± 0.15	1.12 ± 0.15
25°	8.49 ± 1.15(−1)	9.96 ± 1.34(−1)	7.40 ± 0.99(−1)	4.61 ± 0.61(−1)
35°	3.75 ± 0.51(−1)	2.26 ± 0.31(−1)	1.97 ± 0.26(−1)	1.62 ± 0.21(−1)
45°	1.65 ± 0.22(−1)	1.48 ± 0.20(−1)	9.63 ± 1.29(−1)	7.31 ± 0.97(−1)
60°	9.57 ± 1.29(−1)	5.74 ± 0.78(−2)	4.26 ± 0.57(−2)	3.17 ± 0.42(−2)
75°	4.87 ± 0.66(−2)	3.23 ± 0.44(−2)	2.14 ± 0.28(−2)	1.67 ± 0.22(−2)
90°	3.64 ± 0.49(−2)	2.19 ± 0.30(−2)	1.35 ± 1.81(−2)	9.96 ± 1.31(−3)
105°	2.82 ± 0.38(−2)	1.54 ± 0.21(−2)	9.31 ± 1.25(−3)	6.85 ± 0.90(−3)
120°	2.30 ± 0.31(−2)	1.24 ± 1.68(−2)	7.14 ± 0.96(−3)	5.29 ± 0.70(−3)
135°	2.17 ± 0.29(−2)	1.06 ± 1.43(−2)	6.19 ± 0.83(−3)	4.43 ± 0.59(−3)

using the method described below. It can be seen from Figs. 5(a)–5(l) that the DCS smoothly decrease with increasing scattering angle for electron energies above 300 eV. In the energy region between 40 and 300 eV, the cross sections show small shoulders in the angular range between 20° and 60°.

The results of the present work agree with those of Dampc *et al*. [3] for 20 eV electrons within the experimental uncertainties. A comparison at other electron energies was not possible because Dampc *et al*. [3] focused on the measurement of the DCS of THF for lower electron energies.

In general, the present results agree satisfactorily well with the data of Homen *et al*. [5] in the measured energy range for scattering angles higher than 45°. In this angular range, the differences between both data sets are in the order of the experimental uncertainties. The major deviations from the data of Homen *et al*. [5] occur in the angular range between 20° and 35° where the present DCS exhibit small shoulders.

There exist rather large deviations between the present results and those of Milosavljevic *et al*. [1]. Here, the magnitude of the deviation varies with the electron energy. The best agreement was found at 20 and 200 eV, where both data agree within the experimental uncertainties throughout the whole angular range. For electron energies between 60 and 100 eV, both data agree within the experimental uncertainties for scattering angles larger than 35°. Only a poor agreement was found for 30 and 40 eV electrons, where the difference tends to increase with decreasing scattering angle. At 30 eV and 35°, the DCS of Milosavljevic *et al*. [1] is almost three times higher than that of this work.

A better agreement could be found between the results of this work and the data of Colyer *et al*. [2]. In the case of 30 and 40 eV electrons, the present results agree with the data of Colyer *et al*. [2] within the experimental uncertainties except for the scattering angles of 25° and above 120°. For 20 eV electrons, the present results are higher than the data of Colyer *et al*. [2] throughout the whole angular range.

The above comparison reveals that there exist rather large deviations between the experimental results of different groups. They differ not only in the absolute values but also significantly in the angular dependence. The difference in the angular dependence is mostly pronounced at scattering angles around 25°, where the present DCS show shoulders for electron energies below 300 eV, in contrast to those of Milosavljevic *et al*. [1]. In view of the unsatisfactory data situation, a theoretical method is employed in the following to calculate the DCS of THF and to investigate the angular dependence of the DCS including the existence of the shoulders observed at a few angles.

V. THEORETICAL CALCULATION OF DCS OF THF

A few theoretical studies [19–22] have been carried out with respect to the DCS of THF. With the exception of the work of Możejko and Sanche [19] who employed the independent-atom model to calculate the DCS for intermediate and high electron energies, the focus of the studies was placed on the low-energy region below 20 eV. Trevisan *et al*. [20] applied the Kohn method to theoretically determine the DCS of THF for electron energies up to 15 eV. Bouchiha *et al*. [21] calculated the DCS of THF for electron energies below 10 eV using the *R*-matrix method. Winstead and McKoy [22] applied the Schwinger multichannel method for the calculation of DCS of THF for electron energies between 3 and 20 eV.

In the present work, DCS of THF were calculated for electron energies above 60 eV using the modified independent-atom model, which is described in detail by Hayashi and Kuchitsu [23]. It is based on the common independent-atom model, with the difference being that intramolecular multiple-scattering effects are also considered. In the modified independent-atom model, the dominant contribution to the scattering cross section arises from the interaction of the incoming electron wave with the individual atoms comprising the molecule which are assumed to act as independent scattering centers characterized by spherical short-range potentials. Jain [24,25] applied the model for the calculation of the DCS of small linear molecules for electrons in the energy range from 40 to 800 eV and could reach good agreement with experimental data.

In the modified independent-atom model, the contribution by the correlation-polarization potential is coherently added to that of the short-range potential [25]:

$$\frac{d\sigma_{\rm el}}{d\Omega} = |f_L|^2 + 2\,|f_L| \sum_{i=1}^{N_a} |f_i| \cos(\zeta_L - \zeta_i) \frac{\sin\, qR_i}{qR_i} + I_{\rm S} + I_{\rm SS} + I_{\rm SD}^{(1)} + I_{\rm SD}^{(2)} + I_{\rm DD}^{(0)}, \tag{10}$$

$$I_{\rm S} = \sum_{i=1}^{N_a} |f_i|^2, \tag{11}$$

$$I_{\rm SS} = \sum_{i \neq j}^{N_a} f_i^* f_j \sin(qR_{ij})/qR_{ij}, \tag{12}$$

$$q = 2k\, \sin(\theta/2). \tag{13}$$

It should be noted that all the equations in this section are written in atomic units. In Eq. (10), f_L and f_i are the scattering amplitudes due to the correlation-polarization potential and the short-range potential produced by the ith atom of the molecule, respectively. The total number of atoms in the molecule is denoted by N_a. R_i is the distance of the ith atom from the center of mass of the molecule, R_{ij} is the distance between the ith and jth atoms, k is the wave number of the primary electron, and θ is the scattering angle. The quantity ς is the phase shift and is defined by

$$f = |f| \exp(i\zeta). \tag{14}$$

The terms $I_{\rm SD}^{(1)}$, $I_{\rm SD}^{(2)}$, and $I_{\rm DD}^{(0)}$ denote the contributions arising from the intramolecular multiple-scattering effects [23]:

$$I_{\rm SD}^{(1)} = \frac{i}{k} \sum_{i^1 j}^{N} (f_i + f_j)^* \sum_{l_1 l_2 l_3} (2l_1 + 1)(2l_2 + 1)(2l_3 + 1) \times \begin{pmatrix} l_1 & l_2 & l_3 \\ 0 & 0 & 0 \end{pmatrix}^2 P_{l_2}(\cos\theta) j_{l_3}^2(kR_{ij}) A_{l_1}(k,j) A_{l_2}(k,i), \tag{15}$$

$$I_{\mathrm{SD}}^{(2)} = \frac{4\pi i}{k} \sum_{k\neq i\neq j}^{N} f_k^* \sum_{\substack{l_1\ l_2\ l_3\\ l_4\ l_5\ m_3}} i^{l_3-l_4+l_5}(-1)^{m_3} \times (2l_1+1)(2l_2+1)^{1/2}(2l_4+1)(2l_5+1)^{1/2} j_{l_3}^2(kR_{ij}) \times \begin{pmatrix} l_1 & l_2 & l_3 \\ 0 & 0 & 0 \end{pmatrix} \begin{pmatrix} l_1 & l_2 & l_3 \\ 0 & -m_3 & m_3 \end{pmatrix} \begin{pmatrix} l_4 & l_5 & l_3 \\ 0 & 0 & 0 \end{pmatrix} \times \begin{pmatrix} l_4 & l_5 & l_3 \\ 0 & -m_3 & m_3 \end{pmatrix} Y_{l_2,-m_3}(\theta,0) j_{l_4}(kR_{ij}) P_{l_5}(\cos\phi_{jik}) \times j_{l_5}[2kR_{ij}\sin(\theta/2)] Y_{l5,-m_3}\left(\frac{1}{2}\pi - \frac{1}{2}\theta, 0\right) \times A_{l_1}(k,j) A_{l_2}(k,i), \tag{16}$$

$$I_{\mathrm{DD}}^{(0)} = \frac{\pi}{k^2} \sum_{i\neq j} \sum_{l_3} (2l_3+1) j_{l_3}^3(kR_{ij}) \times \sum_{m_3} \left| \sum_{l_1 l_2} (2l_1+1)(2l_2+1)^{1/2} \begin{pmatrix} l_1 & l_2 & l_3 \\ 0 & 0 & 0 \end{pmatrix} \times \begin{pmatrix} l_1 & l_2 & l_3 \\ 0 & -m_3 & m_3 \end{pmatrix} Y_{l_2,-m_3}(\theta,0) A_{l_1}(k,j) A_{l_2}(k,i) \right|^2, \tag{17}$$

$$A_l(k,i) = \exp\left(i\delta_l^{(i)}\right) \sin\delta_l^{(i)}. \tag{18}$$

In Eqs. (15)–(18), j_n is a spherical Bessel function of order n, P_n is a Legendre polynomial, Y_{lm} is a spherical harmonic, ϕ_{ijk} is the angle between the bonding line of the ith, jth, and kth atom, δ_l is the phase shift, and $\left(\begin{smallmatrix} l_1 & l_2 & l_3 \\ m_1 & m_2 & m_3 \end{smallmatrix}\right)$ are the $3j$ symbols.

The scattering amplitude f_i was obtained from the phase shift $\delta_l^{(i)}$ using the partial-wave expansion method:

$$f_i(\theta) = \frac{1}{2ik} \sum_l (2l+1)\left[\exp\left(2i\delta_l^{(i)}\right) - 1\right] P_l(\cos\theta). \tag{19}$$

The phase shift $\delta_l^{(i)}$was calculated by solving the time-independent radial Schrödinger equation

$$\left[\frac{d^2}{dr^2} + k^2 - \frac{l(l+1)}{r^2} - V_{\mathrm{opt}}^{(i)}(r)\right] \varphi_i^{(i)}(kr) = 0 \tag{20}$$

for the ith atom of the molecule with the boundary condition

$$\varphi_l^{(i)}(0) = 0, \quad \varphi_l^{(i)}(r) \to \cos(\delta_l) kr j_l(kr) - \sin(\delta_l) kr n_l(kr) \quad \text{for } r \to \infty, \tag{21}$$

where n_l is a Neuman function.

The complex optical potential V_{opt} is the sum of the short-range electrostatic interaction potential V_{st}, the local exchange potential V_{ex}, and an imaginary absorption potential:

$$V_{\mathrm{opt}}(r) = V_{\mathrm{st}}(r) + V_{\mathrm{ex}}(r) + iV_{\mathrm{abs}}(r). \tag{22}$$

In the present work, the three potentials in Eq. (22) were taken from the paper [26] by Salvat, who described V_{st} in terms of a spherically symmetrical electron density distribution. He used the formulations of Furness and McCarthy [27] for the exchange potential and applied the local-density model in combination with the Born-Ochkur approximation [28,29] to obtain the absorption potential.

In the formulation of the optical potential in Eq. (22), the correlation-polarization potential is omitted because the contribution of the correlation and the polarization effects to the elastic scattering cross section is already taken into account by adding the term $|f_L|^2$in Eq. (10). Assuming that the correlation-polarization potential can be approximated by a spherically symmetrical function due to the random orientation of molecules hit by electrons, the scattering amplitude f_L was calculated again by solving the time-independent radial Schrödinger equation with the corresponding boundary condition described by Eqs. (20) and (21), respectively, where, however, the optical potential V_{opt} was replaced by the correlation-polarization potential V_{pol}.

In defining the correlation-polarization potential, the interaction region was divided into two parts according to the distance R between the incoming electron and the center of mass of the molecule. In the far region, where R is larger than the boundary radius R_b, the definition of which is explained below, it is assumed that V_{pol} arises due to the long-range polarization effect. In this region, V_{pol} was approximated by the Buckingham potential [26]:

$$V_{\mathrm{pol}}(R) = -\frac{\alpha e^2}{2\left(R^2 + R_b^2\right)^2}, \quad R \geqslant R_b, \tag{23}$$

where α is the mean molecular polarizability of THF with a value of 7.9×10^{-24} cm^3 [30].

In the near region where R is so small that the incoming electron interferes with the charge cloud of the molecule, the correlation effect becomes more relevant. Following the suggestion of Padial and Norcross [31], V_{pol} for the near region was defined as

$$V_{\mathrm{pol}}(R) = 0.0311 \ln R_s - 0.0584 + 0.006 R_s \ln R_s - 0.015 R_s \tag{24}$$

for $R_s \leqslant 0.7$ and $R < R_b$,

$$V_{\mathrm{pol}}(R) = -0.07356 + 0.02224 \ln R_s \tag{25}$$

for $0.7 \leqslant R_s \leqslant 10.0$ and $R < R_b$, and

$$V_{\mathrm{pol}}(R) = -0.584 R_s^{-1} + 1.988 R_s^{-3/2} - 2.450 R_s^{-2} - 0.733 R_s^{-5/2} \tag{26}$$

for $R_s \geqslant 10$ and $R < R_b$.

In Eqs. (24)–(26), R_s is given by $R_s = [3/4\pi\rho(R)]^{1/3}$and the boundary radius R_b was defined as the distance between the center of mass of the molecule and that point where the long-range polarization potential given by Eq. (23) crosses the correlation potential described by Eqs. (24)–(26) for the first time. It is worthwhile noting that the permanent dipole moment of THF is not taken into account in the Eqs. (23)–(26).

As Eqs. (10)–(18) indicate, the geometrical arrangement of the atoms within the molecule must be known for the calculation of the DCS. To simplify the calculation, it is assumed that THF has the planar C_{2v} symmetry. For this symmetry, the positions of the atoms and the charge density distribution $\rho(R)$ in the molecule were calculated using the quantum chemical program SPARTAN [32] with the basis set $6-311^{**}$.

VI. RESULTS AND DISCUSSION OF THEORETICAL DCS

The theoretical results of the DCS are represented by the solid lines in Figs. 5(d)–5(l). Good agreement between the experimental and theoretical results was found for electron energies above 400 eV. In this energy range, the differences between the experimental data and theoretical values are in the order of the experimental uncertainties. The greatest deviation was found for the electron energy of 100 eV, where the experimental results are lower than the theoretical values throughout the whole angular range.

For electron energies below 100 eV, the experimental data of Milosavljevic *et al.* [1] are well reproduced by the theoretical values, while the latter are significantly higher than the present experimental results for the scattering angles lower than 45°. The fact that the agreement between theoretical and experimental DCS for electron energies below 100 eV is better than that at the energy of 100 eV is remarkable because the present theoretical method is based on an approximation that is expected to be the better, the higher the energy. It can furthermore be seen from Figs. 5(d))–5(l) that the shoulders observed in the experimental DCS of THF in the angular range between 20° and 60° are qualitatively well reproduced by the theoretical results.

Apart from the accuracy of the theoretical model, deviations between the experimental and theoretical values may, however, arise due to the restriction of the calculation to the planar C_{2v} symmetry. In their study [22], Winstead and McKoy showed that electron scattering by the C_{2v} symmetry can be noticeably different from that by the conformal symmetry C_s and C_2. Gaseous THF can be found in different conformations due to the phenomenon called pseudorotation [33]. Unfortunately, the equilibrium conformation of gaseous THF is not yet exactly known. Spectroscopic [34–36] as well as electron diffraction [37] studies provide contradictory information about the geometry of THF. Recent experimental and theoretical investigations [38,39], however, provide increasing evidence that the mostly populated conformation of gaseous THF has a nonplanar symmetry, i.e., C_2 or C_s.

Figures 6(a) and 6(b) show the relative contribution of each term appearing on the right-hand side of Eq. (10) to the DCS of THF for the electron energies of 100 eV and 1 keV. As can be seen from Figs. 6(a) and 6(b), the greatest contribution originates from the single scattering term I_s, which corresponds to the sum of the DCS of the atoms comprising the molecule. The molecular effect is mainly enclosed in the term I_{ss} that arises due to the coherent scattering of the electron wave by the atoms of the molecules. It depends not only on the scattering amplitude of individual atoms but also on the geometry of the molecule. Note that I_{pol} in Figs. 6(a) and 6(b) is the sum of the relative contribution of the pure polarization and the interference term between the polarization and single scattering, denoted by the first and second terms on the right-hand side of Eq. (10), respectively.

It is evident from Figs. 6(a) and 6(b) that the major contribution to the DCS at low scattering angles arises from the coherent scattering term I_{ss} and the polarization term I_{pol}. At the scattering angles higher than 20°, a significant part of the DCS of THF arises due to the multiple-scattering term $I_{SD}^{(1)}$. In this angular region, $I_{SD}^{(1)}$ has the largest influence on the DCS

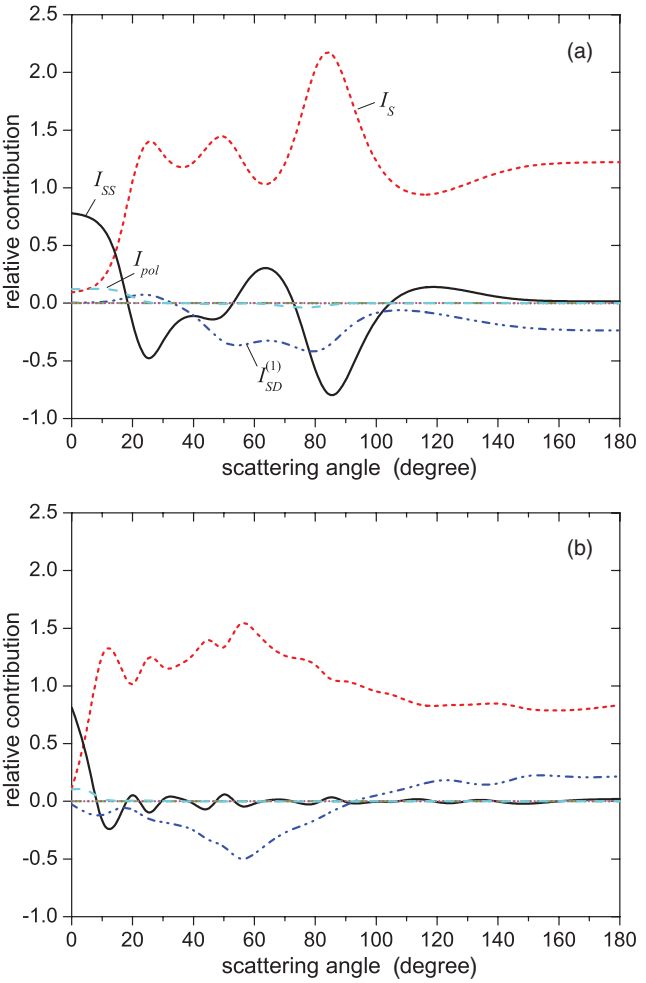

FIG. 6. (Color online) Relative contributions of the scattering terms appearing on the right-hand side in Eq. (10) to the theoretical DCS of THF for two electron energies: (a) 100 eV and (b) 1000 eV. The designation of the line types in (a) also applies to (b).

of THF after the main term I_s for the electron energies above 200 eV. It means that in the case of polyatomic molecules, the disregarding of the multiple-scattering effects may lead to a considerable under- or overestimate of theoretical DCS in a certain angular range even at high electron energies. It should be noted that the relative contribution of the other multiple-scattering terms $I_{SD}^{(2)}$ and $I_{DD}^{(0)}$ are at least two orders of magnitude smaller than that of $I_{SD}^{(1)}$ and, therefore, not shown in Figs. 6(a) and 6(b).

VII. MEASUREMENT OF TCS OF THF

As the apparatus used for the measurement of the TCS has been described in detail in a previous work [40], only a brief description is given here. A schematic view of the experimental setup is depicted in Fig. 7. Electrons produced by heating a hairpin tungsten filament were accelerated to the adjustable energy by a negative voltage applied to the cathode. After being focused by an einzel lens, they passed through two pairs of deflection plates which were placed perpendicularly to each other and used to align the beam direction.

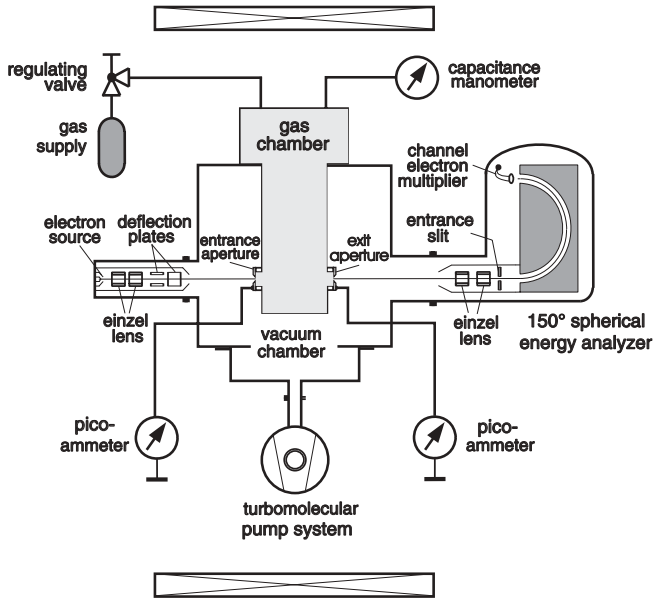

FIG. 7. Schematic view of the experimental setup used for the measurement of TCS of THF.

The electron beam entered the scattering chamber through a circular entrance aperture 0.5 mm in diameter. Electrons that were not scattered or not noticeably deflected by the scattering by the gas molecules leave the chamber through a circular exit aperture also 0.5 mm in diameter. The gas source was provided by liquid THF, whose vapor was introduced into the scattering chamber via a regulating valve. The distance between the midpoint of the entrance and exit aperture was 132 mm. The gas effusing from the scattering chamber through the aperture was evacuated by a turbomolecular pump with a pumping speed of 1500 l/s, which kept the residual pressure in the recipient at lower than 2×10^{-6} mbar.

The pressure in the scattering chamber, which needs to be known absolutely for this experiment, was measured by means of a capacitance manometer. The pressure measurement by means of a capacitance manometer is independent of gas type only in the first order. The so-called thermal transpiration effect can lead to a deviation between its reading and the true value. The height of the deviation depends on the gas type and can be up to 2% in the pressure range of this experiment. Therefore, the manometer was calibrated beforehand at the vacuum metrology section of Physikalisch-Technische Bundesanstalt in Berlin, Germany for several simple gases such as Ar, N_2, and CH_4. In the present work, the calibration data for methane was used to obtain the THF gas pressure from the reading of the capacitance manometer.

The electrons leaving the scattering chamber entered a hemispherical energy analyzer with a mean radius of 100 mm and a deflection angle of 150°. In order to discriminate electrons scattered inelastically in the forward direction, the pass energy of the energy analyzer was set such that only the electrons with the primary beam energy were passed through it. A channel electron multiplier, mounted at the end of the analyzer, was used to detect electrons. The detection solid angle amounted to 7×10^{-3} sr and the relative energy resolution (FWHM) of the analyzer was better than 0.25% so that the fraction of the electrons which had undergone scattering processes but were detected by the channel electron multiplier was negligibly small. Here, the fraction of electrons scattered in the forward direction was estimated using the theoretical method described above. The whole electron-beam path was shielded against the Earth's magnetic field as well as other electromagnetic disturbances by means of a permalloy housing and three orthogonal pairs of Helmholtz coils which actively compensated the major part of the external fields.

As described earlier [40], the TCS for electron energies lower than 20 eV were measured using the 20-eV electron beam and by applying a retarding voltage U_{ret} to the scattering chamber so that electrons undergo scattering processes at the energy $T = 20\ \mathrm{eV} - e|U_{\mathrm{ret}}|$. The determination of the TCS, σ_t, was based on Beer's attenuation law:

$$c = c_0 \exp(-\sigma_t n L), \tag{27}$$

where c_0 and c are the electron count rate measured without and with the gas number density n in the scattering chamber of the length L, respectively. The length L is given by the distance between the midpoint of the entrance and exit aperture of the scattering chamber, which amounted to 132 mm. The gas number density n was calculated using the ideal gas law $n = p/(k_B\Theta)$, where p and k_B are the gas pressure in the scattering chamber and the Boltzmann constant, respectively. The gas temperature is denoted by Θ, which is assumed to be equal to the room temperature.

The electron count rate c was recorded as a function of the gas pressure p which was continuously increased from the residual chamber pressure of about 1.0×10^{-6} mbar to a maximal pressure, depending on the electron energy. The maximal pressure value was chosen such that the beam attenuation did not exceed 60% to avoid multiple-scattering effects. Additionally, the primary electron-beam current I_p was measured on the entrance aperture of the scattering chamber to monitor its possible change due to the exposure of the cathode filament to the gas streaming out through the aperture.

The total scattering cross section was obtained by linearly fitting $\ln[(c/I_p)/(c_0/I_{p,0})]$ versus nL by taking into account the secondary effects described in the previous paper [40], where $I_{p,0}$ is the primary beam current if no gas is present in the scattering chamber. The measurement was repeated ten times for each electron energy to reduce uncertainties arising due to statistical fluctuations. The TCS $\sigma_t(T)$ of THF was determined by multiplying the weighted mean value $\bar{\sigma}_t(T)$ of the ten measurements with three correction factors:

$$\sigma_t(T) = k_1 k_2 k_3 \bar{\sigma}_t(T), \tag{28}$$

where k_1 takes into account the lowering of the experimental TCS due to the finite detector solid angle leading to the counting of elastically scattered electrons, k_2 corrects for the attenuation of the electron beam by the residual gas in the scattering chamber, and k_3 corrects for the widening and displacement of the electron beam by the gas effusing from the scattering chamber through the entrance aperture. The values of the correction factors depend on the electron energy. The maximal value of k_1 and k_3 amounts to 1.01 and 1.002, respectively. The correction factor k_2 was set to unity in the present work but taken into account in the analysis of

TABLE II. Total σ_t, integral elastic σ_{el}, momentum-transfer σ_m, and integral inelastic electron scattering cross sections of THF as a function of the kinetic energy T. The cross sections are given in units of 10^{-16} cm^2. Numbers in parentheses are powers of ten that multiply the cross sections as well as the uncertainties.

	Cross section			
T/eV	σ_t	σ_{el}	σ_m	σ_{inel}
6	56.53 ± 1.95			
8	57.37 ± 1.69			
10	53.89 ± 1.89			
12	52.47 ± 1.84			
14	47.01 ± 1.63			
16	46.35 ± 1.44			
18	47.42 ± 1.48			
20	45.81 ± 1.37			
30	42.26 ± 1.23			
40	39.30 ± 1.14			
60	36.09 ± 0.97	17.70 ± 2.48	5.56 ± 0.78	18.39 ± 2.66
80	33.65 ± 0.87	15.74 ± 2.20	4.20 ± 0.59	17.91 ± 2.37
100	29.13 ± 0.76	15.02 ± 2.07	3.36 ± 0.46	14.11 ± 2.21
200	20.87 ± 0.52	7.52 ± 1.04	1.45 ± 0.20	13.35 ± 1.16
300	16.84 ± 0.42	4.37 ± 0.61	9.01 ± 1.26(−1)	12.47 ± 0.74
400	13.97 ± 0.34	4.22 ± 0.58	5.40 ± 0.74(−1)	9.75 ± 0.67
600	10.54 ± 0.24	3.35 ± 0.47	3.27 ± 0.46(−1)	7.19 ± 0.53
800	8.72 ± 0.19	3.06 ± 0.43	2.39 ± 0.34(−1)	5.66 ± 047
1000	7.55 ± 0.15	2.69 ± 0.37	1.87 ± 0.26(−1)	4.86 ± 0.40

uncertainty. The detailed description of the correction factors and how the weighted mean value was determined is given in Ref. [40]. It should be noted that the additional attenuation of the electron beam in the gas streaming out through the exit aperture of the scattering chamber is taken into account in the calculation of $\bar{\sigma}_t(T)$.

VIII. RESULTS AND DISCUSSION OF THE TCS OF THF

The results of the present measurement are listed in Table II and displayed in Fig. 8 in comparison to those of other experimental groups. Additionally, the TCS obtained by simply adding up those of C_2H_4 [41,42], CH_4 [43], and CO [44–46] are shown in Fig. 9. Note that the combination of the three molecules has the same stoichiometry as THF. It can be seen from Fig. 8 that the present results agree well with those of Możejko *et al.* [7] within the experimental uncertainties. On the contrary, strikingly large deviations occur between the present results and the data of Zecca *et al.* [6]. The former are about 50% higher than the latter. The data of Fuss *et al.* [8] agrees with the present results for electron energies higher than 100 eV within the experimental uncertainties. However, the difference between both data tends to increase with decreasing energy below 100 eV.

In general, the additivity rule of the TCS can only be applied at high electron energies where the Born approximation is valid. It is therefore remarkable that the present results, as can be seen from Fig. 9, agree well with the data obtained using the simple additivity rule for electron energies down to about 40 eV. A noticeable deviation occurs in the energy region around 15 eV, where a dip in the energy dependence of TCS

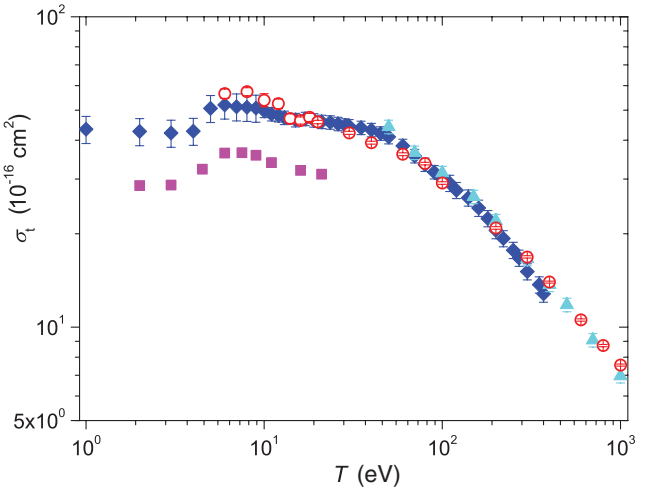

FIG. 8. (Color online) Total electron scattering cross sections of THF as a function of the energy: (◯) present results, (■) Zecca *et al.* [6], (♦) Możejko *et al.* [7], and (▲) Fuss *et al.* [8].

can be observed. A closer look into the energy dependence of the TCS of CO reveals that it is similar to that of THF in the energy region and that this dip might be caused by the C-O bond in THF.

The present TCS of THF was used to determine the integral inelastic scattering cross section σ_{inel} of THF. It was obtained by the subtraction of the integral elastic scattering cross section σ_{el} of THF from the TCS σ_t of THF. The integral elastic scattering cross section was calculated by the integration of the DCS of THF over the scattering angle, where the DCS for scattering angles greater than 135° was obtained by the extrapolation of the experimental data using the angular dependence of the theoretical values shown Figs. 5(d)–5(l). The integral elastic, inelastic, and momentum-transfer cross sections of THF are listed in Table II along with the TCS of THF.

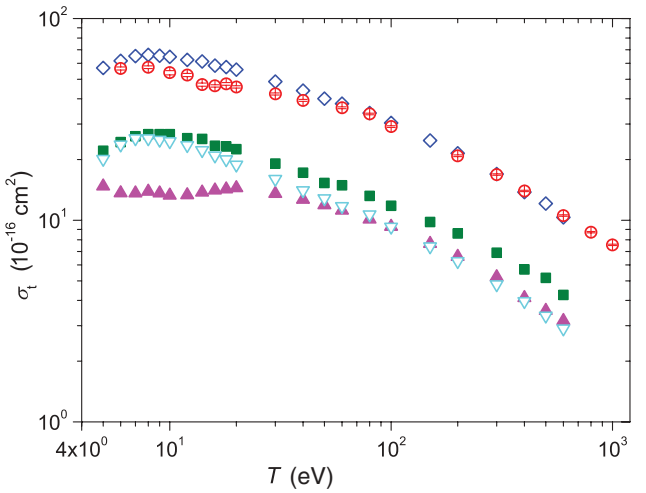

FIG. 9. (Color online) Experimental TCS (◯) of THF in comparison to the values (◇) obtained from the TCS of C_2H_4 (♦) [41,42], CH_4 (▽) [43], and CO (▲) [44–46] using the simple additivity rule.

IX. UNCERTAINTY ANALYSIS

The uncertainties of the DCS were determined in compliance with the *Guide to the Expression of Uncertainty in Measurement* [47]. Since the measuring quantities were not correlated, the standard uncertainty u_{el} of the DCS is given according to the law of propagation:

$$u_{\mathrm{el}}^2 = \left(\frac{\partial\,(d\sigma_{\mathrm{el}}/d\Omega)}{\partial(\eta\Delta\Omega)}u(\eta\Delta\Omega)\right)^2 + \left(\frac{\partial\,(d\sigma_{\mathrm{el}}/d\Omega)}{\partial(\Delta\dot{N})}u(\Delta\dot{N})\right)^2 + \left(\frac{\partial\,(d\sigma_{\mathrm{el}}/d\Omega)}{\partial(\sigma_{\mathrm{tot}})}u(\sigma_{\mathrm{tot}})\right)^2 + \left(\frac{\partial\,(d\sigma_{\mathrm{el}}/d\Omega)}{\partial(\Delta I)}u(\Delta I)\right)^2. \tag{29}$$

As described above, the detection efficiency η and the solid angle $\Delta\Omega$ are correlated via Eqs. (6) and (7). Therefore, the uncertainty of the solid angle $\Delta\Omega$ was embedded in that of the product $\eta\Delta\Omega$. The uncertainty of the detection efficiency η is comprised of that of the quantities appearing in Eq. (7):

$$u^2(\eta) = \left[\frac{\partial\eta}{\partial\hat{\eta}_1}u(\hat{\eta}_1)\right]^2 + \left[\frac{\partial n}{\partial\hat{\eta}_2}u(\hat{\eta}_2)\right]^2 + \left[\frac{\partial\eta}{\partial\eta(T=20\ \mathrm{eV})}\Delta\eta(T=20\ \mathrm{eV})\right]^2. \tag{30}$$

According to the scaling law in charged particle optics, the electron path should be independent of energy in the first order if the ratio of the kinetic energy to the path-influencing potentials is kept constant. A deviation from this law may, however, arise due to fringing electric fields and contact potentials between metallic components of the energy analyzer. In this work, $u[\hat{\eta}_1(T)]/\hat{\eta}_1(T)$ was estimated by means of the difference between the pass-energy dependence of the width (FWHM) of the experimental elastic scattering peak and that of the calculated one. This difference amounted to 7%. A representative example of the pass-energy dependence of the peak width is shown in Figs. 1(a) and 1(b). The relative uncertainty $u[\hat{\eta}_2(T)]/\hat{\eta}_2(T)$ of the detector responsitivity was 5%.

According to Eq. (6), the uncertainty of the detection efficiency $\Delta\eta(T = 20\ \mathrm{eV})$ for 20 eV electrons consists of that of the count rate $\Delta\dot{N}_{\mathrm{el}}(\theta, T = 20\ \mathrm{eV})$ of the elastic scattering peak, of the current loss ΔI at that energy, and that of the uncertainty of the data of Register *et al.* [13] used for the extrapolation of $\Delta\dot{N}_{\mathrm{el}}(\theta, T = 20\ \mathrm{eV})/d\Omega$ for He to scattering angles below 15° and above 135°. These uncertainty sources lead to a relative uncertainty of 8% for $\Delta\eta(T = 20\ \mathrm{eV})$. It is worthwhile mentioning that the uncertainties of the DCS of He by Register *et al.* [13] do not fully enter into $\Delta\eta(T = 20\ \mathrm{eV})$ because not their absolute values but only their angular dependence was used for the extrapolation of $\Delta\dot{N}_{\mathrm{el}}(\theta, T = 20\ \mathrm{eV})/d\Omega$ to a limited angular range. The application of Eq. (30) then yields 11.7% for the relative uncertainty of $u[\eta(T = 20\ \mathrm{eV})]$. The uncertainty of the detector count rate $\Delta N(\theta, T)$ is of a statistical nature and varies between 0.5% and 3% depending on the electron energy and scattering angle.

In general, the current measurement with a Faraday cup is impacted by the counting of secondary electrons released by primary electrons hitting metallic surfaces, by backscattering of the incident particles, and noise and nonlinearity of the electrometer connected to the Faraday cup. The uncertainty due to secondary electron emission and backscattering was determined by the measurement of the current change while varying the voltages applied to the electrostatic guide rings and the Faraday cup. It was estimated as 6% where the uncertainty arising due to the current fluctuation when changing the scattering angle is included. The uncertainty of the reading of the electrometer was set to be equal to that of the calibration, which was lower than 1%. The contribution of a noise or leakage current to the uncertainty was set to zero because they subtract away when calculating the current loss. The relative standard uncertainty of the DCS calculated using Eq. (29) varies between 13% and 15% depending on the electron energy and scattering angle.

The uncertainty analysis for the TCS is omitted here since the uncertainty sources and their contributions to the standard uncertainty of σ_t are almost the same as described in detail in Ref. [40], apart from the unknown calibration factor of the capacitance manometer for THF. As mentioned above, the calibration factor for methane was used to determine the pressure of THF in the scattering chamber from the reading of the capacitance manometer. It is assumed that this approach leads to a calibration uncertainty for THF twice that for methane. The relative standard uncertainty of the TCS therefore lies between 2% and 3.5%.

X. CONCLUSION

Applying a new experimental technique, differential elastic scattering cross sections of THF were measured absolutely for electrons in the energy range from 20 eV to 1 keV with experimental uncertainties between 13% and 15%. Although significant deviations were found between the experimental results of different groups, there are no systematic differences between the present results and the experimental data of other groups that were obtained using the relative flow technique [10]. The present results even agree well with those of other groups at several energies, suggesting that the relative flow technique is also appropriate for the measurement of DCS of polyatomic molecules with high dipole moments.

The large deviations among the experimental results of different groups not only in the magnitude but also in the angular dependence demonstrate that the current data situation for the DCS of THF is not satisfactory and additional experimental investigations are required to clarify the existing large deviations. The modified independent-atom model seems to be an appropriate approach for the calculation of the DCS of polyatomic organic molecules for electron energies above 60 eV. The theoretical DCS of THF calculated using this model agree qualitatively well with the present experimental results.

Total scattering cross sections of THF were measured for electron energies between 6 eV and 1 keV with experimental uncertainties between 2% and 3.5%. The results of the present experiment agree with those of Możejko *et al.* [7] within the experimental uncertainties, but relative deviations in the order

of 50% were found between the present results and the data of Zecca *et al*. [6]. Therefore, supplemental studies with respect to the TCS of THF are also to be suggested.

APPENDIX

Equations (1) and (2) can be extended to the measurement of doubly differential scattering cross sections:

$$\frac{d[\Delta\dot{N}(\theta,T)]}{dE} = \eta(E)\frac{d^2\sigma(\theta,T)}{dE\,d\Omega}V_{\text{eff}}, \tag{A1}$$

where E is the energy of the scattered electrons and $\eta(E)$ is the energy-dependent detection efficiency. The apparatus used in the present work was arranged such that the relative variation of the solid angle $\Delta\Omega(\vec{r})$ over the interaction area is smaller than 0.2%. This was achieved simply by making the distance between the interaction area and the entrance slit of the energy analyzer large compared to the width of the molecular beam so that the interaction area nearly appears as a point source. Furthermore, the maximal change of the scattering angle over the interaction area was 0.3°, so that $G[\theta'(\vec{r})]$ was set to unity. The uncertainties arising due to the disregard of the variation of $G[\theta'(\vec{r})]$ are much smaller than those caused by other sources, except scattering angles below 5°.

Since the change of the solid angle can be neglected, $\Delta\Omega(\vec{r})$ can be extracted from the integral in Eq. (2):

$$V_{\text{eff}} \approx \Delta\Omega\int_V i(\vec{r})f(\vec{r})d\vec{r} \equiv \Delta\Omega V'_{\text{eff}}. \tag{A2}$$

The insertion of Eq. (A2) into Eq. (A1) yields

$$\frac{1}{\eta(E)}\frac{d}{dE}\left(\frac{\Delta\dot{N}}{\Delta\Omega}\right) = V'_{\text{eff}}\frac{d^2\sigma}{dE\,d\Omega}. \tag{A3}$$

The integration of both sides of Eq. (A3) over the scattering angle and the secondary electron energies gives

$$\int\frac{1}{\eta(E)}\frac{d}{dE}\left(\frac{\Delta\dot{N}}{\Delta\Omega}\right)dE\,d\Omega = \int\frac{d^2\sigma}{dE\,d\Omega}V'_{\text{eff}}\,dE\,d\Omega. \tag{A4}$$

Since V'_{eff} does not depend on the energy of scattered electrons and on the scattering angle, Eq. (A4) can be written as

$$\int\frac{1}{\eta(E)}\frac{d(\Delta\dot{N})}{dE\,\Delta\Omega}dE\,d\Omega = V'_{\text{eff}}\int\frac{d^2\sigma}{dE\,d\Omega}dE\,d\Omega. \tag{A5}$$

The left-hand side in Eq. (A5) corresponds to the total number $\dot{N}$ of electrons scattered per second and the integral on the right-hand side is equal to the total scattering cross section σ_t:

$$\dot{N} = V'_{\text{eff}}\sigma_t. \tag{A6}$$

Due to the conservation of the particle number, $\dot{N}$ has to correspond to the current loss ΔI of the primary electron beam in the forward direction:

$$\dot{N} = \frac{\Delta I}{e}, \tag{A7}$$

where e is the electron charge. It follows from Eqs. (A6) and (A7):

$$V'_{\text{eff}} = \frac{\Delta I}{e\sigma_t}. \tag{A8}$$

The insertion of Eq. (A8) into Eq. (A3) gives

$$\frac{d^2\sigma}{d\Omega\,dE} = \frac{e}{\eta(E)}\frac{d}{dE}\left(\frac{\Delta\dot{N}}{\Delta\Omega}\right)\frac{\sigma_t}{\Delta I}. \tag{A9}$$

In the case of elastic scattering, the energy E of scattered electrons is equal to the primary energy T, and Eq. (A9) reduces to

$$\frac{d\sigma(\theta,T)}{d\Omega} = \frac{e}{\eta(T)}\frac{\Delta\dot{N}(\theta,T)}{\Delta\Omega}\frac{\sigma_t(T)}{\Delta I}. \tag{A10}$$

[1] A. R. Milosavljevic, A. Giuliani, D. Sevic, M.-J. Hubin-Franskin, and B. P. Marinkovic, Eur. Phys. J. D **35**, 411 (2005).
[2] C. J. Colyer, V. Vizcaino, J. P. Sullivan, M. J. Brunger, and S. J. Buckman, New J. Phys. **9**, 41 (2007).
[3] M. Dampc, A. R. Milosavljevic, I. Linert, B. P. Marinkovic, and M. Zubek, Phys. Rev. A **75**, 042710 (2007).
[4] M. Allan, J. Phys. B **40**, 3531 (2007).
[5] M. G. P. Homem, R. T. Sugohara, I. P. Sanches, M. T. Lee, and I. Iga, Phys. Rev. A **80**, 032705 (2009).
[6] A. Zecca, C. Perazzolli, and M. J. Brunger, J. Phys. B **38**, 2079 (2005).
[7] P. Możejko, E. Ptasińska-Denga, A. Domaracka, and C. Szmytkowski, Phys. Rev. A **74**, 012708 (2006).
[8] M. Fuss, A. Muñoz, J. C. Oller, F. Blanco, D. Almeida, P. Limão-Vieira, T. P. D. Do, M. J. Brunger, and G. García, Phys. Rev. A **80**, 052709 (2009).
[9] R. T. Brinkmann and S. Trajmar, J. Phys. E **14**, 245 (1981).
[10] S. K. Srivastava, A. Chutjian, and S. Trajmar, J. Chem. Phys. **63**, 2659 (1975).
[11] S. J. Buckman and R. J. Gulley, Meas. Sci. Technol. **4**, 1143 (1993).
[12] A. E. Hughes and C. C. Phillips, Surf. Interface Anal. **4**, 220 (1982).
[13] D. F. Register, S. Trajmar, and S. K. Srivastava, Phys. Rev. A **21**, 1134 (1980).
[14] A. Jablonski, F. Salvat, and C. J. Powell, *NIST Electron Elastic-Scattering Cross-Section Database* (US Department of Commerce, Gaithersburg, MD, 2003).
[15] M. P. Seah, J. Electron Spectrosc. Relat. Phenom. **50**, 137 (1990).
[16] H. K. Holt and R. Krotkov, Phys. Rev. **144**, 82 (1966).
[17] A. L. Sinfailam, J. Phys. B **9**, L101 (1976).
[18] L. Boesten and H. Tanaka, At. Data. Nucl. Data Tables **52**, 25 (1992).
[19] P. Możejko and L. Sanche, Radiat. Phys. Chem. **73**, 77 (2005).

[20] C. S. Trevisan, A. E. Orel, and T. N. Rescigno, J. Phys. B **39**, L255 (2006).
[21] D. Bouchiha, J. D. Gorfinkel, L. G. Caron, and L. Sanche, J. Phys. B **39**, 975 (2006).
[22] C. Winstead and V. McKoy, J. Chem. Phys. **125**, 074302 (2006).
[23] S. Hayashi and K. Kuchitsu, J. Phys. Soc. Jpn. **41**, 1724 (1976).
[24] A. Jain, J. Phys. B **15**, 1533 (1982).
[25] A. Jain and S. S. Tayal, J. Phys. B **15**, L867 (1982).
[26] F. Salvat, Phys. Rev. A **68**, 012708 (2003).
[27] J. B. Furness and I. E. McCarthy, J. Phys. B **6**, 2280 (1973).
[28] V. I. Ochkur, Sov. Phys. JETP **18**, 503 (1964).
[29] V. I. Ochkur, Sov. Phys. JETP **20**, 1175 (1965).
[30] D. W. Davidson, R. N. O'Brien, P. Saville, and S. Visaisouk, J. Opt. Soc. Am. B **3**, 864 (1986).
[31] N. T. Padial and D. W. Norcross, Phys. Rev. A **29**, 1742 (1984).
[32] SPARTAN '08, Wavefunction, Inc., Irvine, CA.
[33] J. E. Kilapatrick, K. S. Pitzer, and R. Spitzer, J. Am. Chem. Soc. **69**, 2483 (1947).
[34] G. G. Engerholm, A. C. Luntz, W. D. Gwinn, and D. O. Harris, J. Chem. Phys. **50**, 2446 (1969).
[35] R. Meyer, J. C. Lopez, J. L. Alonso, S. Melandri, P. G. Favero, and W. Caminati, J. Chem. Phys. **111**, 7871 (1999).
[36] A. H. Mamleev, L. N. Gunderova, and R. V. Gallev, J. Struct. Chem. **42**, 365 (2001).
[37] H. J. Geise, W. J. Adams, and L. S. Bartell, Tetrahedron **25**, 3045 (1969).
[38] V. M. Rayon and J. A. Sordo, J. Chem. Phys. **122**, 204303 (2005).
[39] T. C. Yang, G. L. Su, C. G. Ning, J. K. Deng, F. Wang, S. F. Zhang, X. G. Ren, and Y. R. Huang, J. Phys. Chem. A **111**, 4927 (2007).
[40] W. Y. Baek and B. Grosswendt, J. Phys. B **36**, 731 (2003).
[41] O. Sueoka and S. Mori, J. Phys. B **19**, 4035 (1986).
[42] P. Wickramarachchi, P. Palihawadana, G. Villela, and W. M. Ariyasinghe, Nucl. Instrum. Methods Phys. Res. B **267**, 3391 (2009).
[43] B. Grosswendt and W. Y. Baek, L.N.L.-I.N.F.N. Report No. 161, 2000 (unpublished).
[44] I. Kanik, J. C. Nickel, and S. Trajmar, J. Phys. B **25**, 2189 (1992).
[45] C. K. Kwan, Y. F. Hsieh, W. E. Kauppila, S. J. Smith, T. S. Stein, M. N. Uddin, and M. S. Dababneh, Phys. Rev. A **27**, 1328 (1983).
[46] G. Garcia, C. Aragon, and J. Campos, Phys. Rev. A **42**, 4400 (1990).
[47] International Organization for Standardization (ISO), *Guide to the Expression of Uncertainty in Measurement* (ISO, Geneva, 1993).